This version of the article has been accepted for publication, after peer review but is not the Version of Record and does not reflect post-acceptance improvements, or any corrections. The Version of Record is available online at: https://doi.org/10.1007/s00170-024-14214-2.

Use of this Accepted Version is subject to the publisher's Accepted Manuscript terms of use https://www.springernature.com/gp/open-research/policies/accepted-manuscript-terms

Large-format Material Extrusion Additive Manufacturing of PLA, LDPE, and HDPE compound feedstock with spent coffee grounds

***Alessia Romani*[1,2,*,A], *Martina Paramatti*[1,A], *Laura Gallo*[3], *Marinella Levi*[1]**

[1] Department of Chemistry, Materials and Chemical Engineering "Giulio Natta", Politecnico di Milano – Via Durando 38/A, 20158 Milano, Italy

[2] Design Department, Politecnico di Milano – Via Durando 38/A, 20158 Milano, Italy

[3] CoffeeFrom S.r.l. – Via Del Corso 1, 20122 Milano, Italy

* Corresponding author: Alessia Romani, 10439844@polimi.it

[A] These authors equally contributed to the work.

Abstract

As an abundant commodity, coffee production generates significant scraps and by-products, increasing the potential pollution hazards. Circular economy and bioeconomy can help valorize Spent Coffee Grounds (SCGs), e.g., as fillers in polymer-based composites using conventional manufacturing, i.e., injection molding. Large-format additive manufacturing with pellet extruders offers a further option for new applications, reducing costs for the valorization of biomass waste. However, its use in this context remains unexplored, especially for applications with complex geometries or critical overhangs. This work investigates new biomass waste-based materials for large-format additive manufacturing with direct feeding extrusion, fabricating self-supported complex overhang geometries through nonplanar slicing. The thermal, rheological, and mechanical properties of three novel polymer-based pellet compounds with post-industrial SCGs, i.e., injection molding grade polylactic acid/SCGs, recycled low-density polyethylene/SCGs, and high-density polyethylene/SCGs, were herein investigated to evaluate their printability, defining their extrusion temperatures (190°C and 170°C). Results showed suitable viscosity ranges (133.6-839.7 Pa·s) and accurate tensile values comparable with literature, e.g., ~1-3% minimum relative standard deviations (polylactic acid/SCGs), or conventional manufacturing, e.g., elastic moduli of 107.4 MPa (recycled low-density polyethylene/SCGs) and 587 MPa (high-density polyethylene/SCGs). Their use with large-format 3D printers was assessed thanks to nonplanar samples with complex overhang geometries, reaching a maximum curvature angle of 32° and fabricating overhangs up to 25° without supports. According to the tests, especially polylactic acid/SCGs, a bio-based compound, and recycled low-density polyethylene/SCGs, a fully recycled material, can be used for large-format 3D printing applications with complex geometries, e.g., furniture, interior, and exhibition design. This work paves the way for new materials for large-format additive manufacturing, reducing the need for 3D printing grade feedstock, cutting costs and consumption from filament processing, and fostering material waste reduction practices.

Keywords

3D printing, bio-based polymer compound, Fused Granular Fabrication, Fused Filament Fabrication, Circular economy, nonplanar slicing

Introduction

In the last decades, generating food waste and loss has arisen as a global issue to be mitigated through collaborative practices between institutions, policymakers, industries, and citizens [1, 2]. In 2019, 931 million tons of food waste were produced at a global level, which means the 17% of the total food production [1]. Food waste in landfills contributes from 8 to 10% of global greenhouse gas emissions, affecting climate change and world hunger[1, 3]. Although prevention is the most preferred option, valorization strategies for discarded food, such as optimization, recycling, and recovery, can significantly help foster sustainable practices against food waste, especially for abundant commodities and, consequently, potential waste.

For instance, coffee, the second most consumed beverage globally, reached a total production of 170.8 million of 60 kg bags in 2021 [4, 5]. Due to its widespread consumption, it faces environmental, economic, and societal challenges through its production value chain. Coffee production generates different kinds of scraps and waste, such as pulp, husk, silver skin, and spent coffee grounds, causing up to 2 billion tons of agro-waste per year [6]. Spent Coffee Grounds (SCGs) represent one of the most significant scraps from coffee production and consumption, representing 90% of the initial coffee bean mass [7]. Their improper disposal of these scraps may lead to potential pollution hazards, moving away from implementing sustainable production and consumption models, i.e., circular economy and bioeconomy [8].

Circular economy aims to create closed- or open-loops of resource flows to keep in use through time, retaining their value as long as possible without the need for further loops [9, 10]. Its principles, i.e., reuse and recycle, are implemented thanks to circular value chains, as opposed to linear take-make-waste models [11], fostering new practices amongst stakeholders, i.e., industrial symbiosis [12]. Similarly, the bioeconomy also focuses on resource flows to promote sustainable models of production and consumption [13]. In detail, bioeconomy practices rely on renewable biological resources as the main source of new energy and goods [14, 15]. To this end, handling material flows plays a crucial role in fostering circular economy and bioeconomy practices, and several strategies can be adopted by researchers and industrial stakeholders, e.g., studying new manufacturing processes [16, 17], reducing waste, or keeping scraps and by-products in use [13, 18].

The valorization of biomass scraps and by-products shows promising pathways to combine circular economy principles and bioeconomy for new sustainable models [19, 20], including natural fibers [16] and bio-based secondary raw materials from the food sector, e.g., soybean hulls [21, 22], coconut scraps [23, 24], or SCGs [4, 6]. Focusing on SCGs, circular bioeconomy strategies may include their use as food and drug ingredients, compost, bioenergy recovery, or in new consumer goods and constructions [25, 26]. In the latter case, SCGs can be used for new composite materials, i.e., polymer-based composites, valorizing the bio-based scraps as fillers for new compounds. From the literature, polylactic acid (PLA), polypropylene (PP), and polyethylene (PE) are used as matrixes for polymer-based composites filled with SCGs, obtaining new compounds with tunable characteristics, i.e., enhanced mechanical properties [27, 28], or fully bio-based formulations, i.e., PLA/SCGs [29].

These SCGs composites can be processed through different manufacturing processes, such as extrusion, compression molding, and injection molding, reaching a broad range of applications, i.e., food packaging [29, 30]. Recently, new feedstock materials containing SCGs have been studied by using other processing technologies, widening their potential uses in circular bioeconomy contexts. Among those, Additive Manufacturing (AM), in particular Material Extrusion (MEX) processes [31], stands out as a viable option for the valorization of SCGs, especially considering PLA/SCGs formulations [32, 33]. As a matter of fact, MEX processes allow the use of different material feedstock, including thermoplastic and thermoset polymer-based composites for structural applications [16, 34], as well as bio-based or recycled raw materials [35, 36]. However, recent works are mainly focused on small-format Fused Filament Fabrication (FFF, also known as Fused Deposition Modeling, FDM), which needs further reprocessing steps to allow the use of secondary raw materials, i.e., extruding 3D printing filaments. The use of large-format AM (LFAM, also Large-scale AM, LSAM) systems equipped with pellet extrusion systems for granulate feedstocks (Fused Granular Fabrication, FGF, or Fused Particle

Fabrication, FPF) can potentially enlarge the range of applications by producing bigger parts [37, 38]. Moreover, FGF AM systems reduce processing costs and offer a wider choice of materials, i.e., less expensive compounded pellets for conventional processes or direct mixing of new formulations in the pellet extrusion system [39, 40]. Despite the increasing interest in reprocessing biomass waste through AM, the use of LFAM FGF 3D printers with biomass scraps or by-products is still limited [41], as well as the range of biomass waste-based polymer blends available for large-scale FGF AM processes. For instance, most biomass waste-filled feedstock is currently used with small-scale 3D printing systems or produced in the form of filaments, which are not optimal for processes dealing with bigger volume parts and higher material consumption [18, 41]. For this reason, relying on granulated compound feedstocks from other processes, e.g., injection molding, can speed up the adoption of new biomass waste-filled materials for LFAM, increasing their availability for real-world applications.

However, LFAM entails some intrinsic drawbacks, especially when considering gantry- or delta-based systems. First, high-resolution parts with intricated geometries or overhangs can be challenging, especially considering the typical nozzle dimensions and layer height thicknesses [42, 43]. Supports are also scarcely used or avoided in LFAM, representing a significant source of material waste, increasing 3D printing times, and being difficult to remove without damaging the part. Furthermore, ensuring good shape retention, interlayer adhesion, and consistency of the extrudate means achieving optimal control of the temperatures during the whole fabrication process, including cooling times [44, 45]. For example, overhangs with critical angles tend to collapse during 3D printing due to the increased cooling times and thicker layers, requiring heat transfer optimization [45, 46]. To this end, non-conventional fabrication methods and processes can be used to broaden the range of achievable geometries, i.e., nonplanar slicing. This strategy consists of moving the extruder head on the z-axis during the deposition of the single layers, resulting in 3D nonplanar paths instead of 2D layer sections [47, 48]. Although similar strategies are currently used for robot-based AM to define feasible trajectories and avoid collapses, they can also be used with gantry- or delta-based systems to improve surface quality and dimensional accuracy, reducing 3D printing times, and optimizing the gcode [47, 49]. When combined with LFAM, this slicing technique allows for fabricating more complex shapes by reducing the overhang angle of a specific geometrical feature through custom 3D layer paths. Its use with LFAM can, therefore, improve the shape retention of final parts, reducing collapses and processing a wider range of materials by improving the overall quality, e.g., less conventional granulates or pellets not specifically produced for 3D printing processes. From the literature, there are very few works showing 3D printed complex geometries, as well as sample applications, with both LFAM FGF 3D printers and polymer-based feedstocks from biomasses or scraps [41, 50]. Only one study narrows the investigation to specific 3D printing grade PLA/SCGs granulates [51], which can be scarcely available and more expensive compared to pellet feedstock for conventional manufacturing processes [40, 43]. To the best of the authors' knowledge, no previous work focused on biomass- and polymer-based pellet compounds from conventional processes, such as injection molding, nor considered other matrixes besides PLA with large-format FGF AM apparatuses to fabricate parts with critical overhangs without requiring supports, or with nonplanar slicing techniques, e.g., for potential product applications

This work widens the available biomass waste-based materials for LFAM FGF extrusion systems by investigating the use of polymer-based pellet compounds filled with post-industrial SCGs from conventional processes, i.e., injection molding. In detail, this work explores the printability of SCGs-based polymer compounds for potential applications, aiming to fabricate 3D printed self-supported complex geometries by combining nonplanar slicing and LFAM FGF apparatuses. The printability assessment of three different injection molding grade compounds, i.e., polylactic acid (PLA), recycled low-density polyethylene (LDPE), and high-density polyethylene (HDPE) filled with 10% wt. of SCGs, was conducted in this work by carrying out Differential Scanning Calorimetry (DSC), rheological flow stress ramp tests, and tensile tests. After assessing the overall 3D printing quality of the tensile specimens, some 3D samples were 3D printed with nonplanar slicing techniques, which means using curvilinear extrusion paths in the z-axis, to validate the use of the three commercial injection molding grade compounds with large-format AM technologies. LFAM FGF can potentially enlarge the range of applications of commercial biomass-based or fully recycled composites from scraps or by-products, i.e., SCGs thermoplastic compounds, without the need for further reprocessing steps and energy

consumption to obtain new secondary raw materials for 3D printing, such as extruding filaments, paving the way for large-format applications with significant cost save.

Materials and Methods

Materials and experimental workflow

This work studied three commercial formulations of polymer compounds filled with a constant weight percentage of SCGs, including composite materials with bio-based or recycled matrixes: PLA/SCGs, rLDPE/SCGs, and HDPE/SCGs. These compounds are usually processed through injection molding; hence, they are not primarily formulated for extrusion or FFF/FGF AM processes. PLA/SCGs consist of a PLA matrix filled with 10% wt. of SCGs from post-industrial scraps. rLDPE/SCGs is made of a recycled LDPE matrix from post-industrial recycled material filled with 10% wt. of SCGs. HDPE/SCGs consist of an HDPE matrix filled with 10% wt. of SCGs. The three formulations were compounded by Nexeo Plastics Italy S.r.l. (Milano, Italy) and supplied in the form of pellets used as received as feedstocks for the large-format FGF 3D printer. PLA/SCGs compound was selected as a starting point for the experimentation, as PLA is a well-established polymer for FFF/FGF [52]. rLDPE and HDPE compounds were chosen to widen the range of available materials for FFF/FGF AM, currently representing challenging matrixes to be processed through MEX AM processes, especially with large-format systems. The workflow and the characterization techniques of this study are resumed in Figure 1. DSC and rheology tests were conducted on the three pellet feedstock, whereas 3D printed specimens were fabricated for the tensile tests and to evaluate the printability of complex geometries, i.e., from nonplanar slicing techniques.

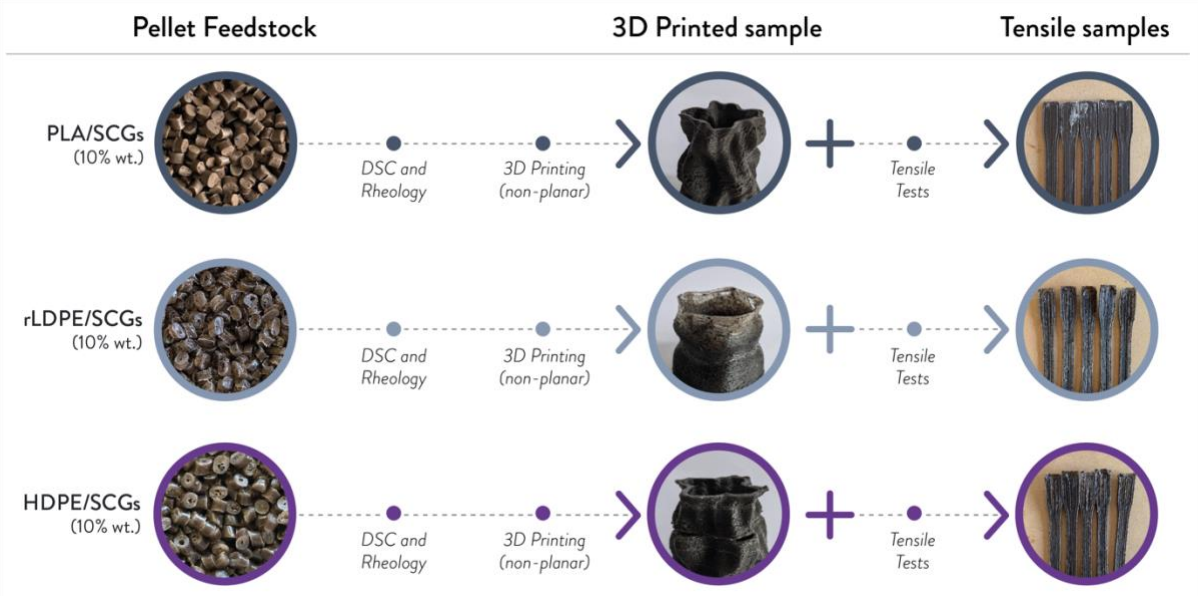


Fig. 1 – Experimentation workflow with the different formulations (PLA/SCGs, rLDPE/SCGs, HDPE/SCGs) and characterization tests.

Materials characterization

Differential Scanning Calorimetry (DSC) was used to evaluate the glass transition temperature (T_g), the cold crystallization temperature (T_{cc}), the enthalpy of cold crystallization (ΔH_{cc}), the melting temperature (T_m), and the enthalpy of fusion (ΔH_m) of the three formulations. Tests were performed with a Mettler-Toledo DSC/823e machine (Mettler Toledo, Columbus, OH, US), using 10-20 mg samples of PLA/SCGs, rLDPE/SCGs, and HDPE/SCGs. The samples underwent three thermal cycles, i.e., heating-cooling-heating, at 20°C/min scan rates, defining the temperature ranges for the tests according to literature and the processing temperatures recommended by the supplier of the specific formulations

[28, 51]. For PLA/SCGs, the first heating scan was from 25 to 220°C, the cooling scan from 220 to -50°C, and the second heating scan from -50 to 220°C. rLDPE/SCGs and HDPE/SCGs underwent a first heating scan from 20 to 200°C, a cooling scan from 200 to 20°C, and a second heating scan from 20 to 200°C. The degree of crystallinity (χ) was calculated for the PLA/SCGs, rLDPE/SCGs, and HDPE/SCGs formulations according to Equation 1:

$$\chi = \frac{\Delta H_m}{\Delta H_m^0} 100 \quad \text{Eq. 1}$$

where ΔH_m is the normalized enthalpy of fusion, and ΔH^0_m is the standard fusion enthalpy for purely crystalline materials reported in the literature, which means 93.1 J/g for PLA [53] and 293 J/g for LDPE and HDPE [54].

Flow ramp tests were carried out with a Discovery HR-2 hybrid rheometer (TA Instruments Inc., New Castle, DE, US) to evaluate the viscosity values as a function of the shear rate, simulating the processing conditions of the extruder chamber, i.e., by choosing the extrusion temperature (Table 1). Rheological tests were done on the pellets of the three formulations with a 25 mm parallel steel plate geometry at 190°C (PLA/SCGs) and at 170°C (rLDPE/SCGs, HDPE/SCGs) for 180 s with a gap of 500 µm, applying a shear rate ranging from 10^{-2} to 10^{2} s^{-1}. The results were plotted on a log-log graph and were used to calculate the viscosity values when the shear rate is 10 s^{-1}, corresponding to the feed rate used in this work, i.e., 10 mm/s [55]. The reference shear rate was calculated using Equation 2:

$$\dot{\gamma}_w = \frac{\pi D N}{60 H} \quad \text{Eq. 2}$$

where $\dot{\gamma}_w$ is the expected shear rate in the internal screw channel wall of the extruder chamber, D is the screw diameter in mm, N is the screw speed expressed in rps, and H is the channel depth of the extruder chamber in mm [56]. The results were discussed also considering the Melt Flow Index (MFI) values of the three commercial pellet feedstocks.

The stress-strain curves of the three formulations were obtained through tensile tests with a ZwickRoell Z010 testing machine (ZwickRoell GmbH & Co. KG, Ulm, Germany). The machine was equipped with a 10 kN load cell and square grips. At least five Type I 3D printed samples for each compound were tested according to the ASTM D638-22 standard [57]. To ensure compliance with the testing times provided by the standard, the samples were tested at a speed of 1 mm/min for PLA/SCGs specimens and 5 mm/min for rLDPE/SCGs and HDPE/SCGs samples, which have a thickness of 3 mm, a width of 13 mm, and a nominal gauge length of 57 mm. The speed for each formulation was selected according to the recommended values for rigid and semirigid plastics provided by the ASTM standard, ensuring the rupture in a range between 0.5 and 5 min from the start of the tensile test [57]. The mean values, the standard deviations, and the relative standard deviations of elastic modulus (E), yield strength (σ_y), ultimate tensile strength (σ_m), fracture strength (σ_b), elongation at maximum strength (ε_m), and elongation at break (ε_b) were calculated starting from the experimental results.

3D printing setup and tests

A Delta Wasp 3MT Industrial (Wasp S.r.l., Massa Lombarda, Italy) was used to 3D print the SCGs composites. This 3D printer is a large-format Fused Granular Fabrication (FGF) delta-based system with a maximum building volume of 1 m^3 equipped with a circular stainless steel bed and a single screw pellet extruder (Figure 2a), which allows the direct feeding and extrusion of granulate or pellet thermoplastics and composites [37]. The extruder is equipped with a Ø3mm stainless steel nozzle.

Preliminary 3D printing tests were carried out to define the specific 3D printing parameters for the selected LFAM FGF system and evaluate the quality and consistency of the extrudates, which means (a) extrusion-only gcodes and (b) 3D-printed vase mode cylinders with an overall dimension of 100x100x140 mm. Two kinds of samples were 3D printed to assess the quality of the process: (a) tensile test specimens with conventional planar slicing and (b) 3D samples with nonplanar slicing techniques. The 3D printing parameters to fabricate the tensile specimens and the 3D samples are shown in Table

1. The extruder and bed temperatures were selected according to the specific compound pellet feedstocks, the thermal analysis, and the average temperatures used for processing similar materials and matrixes with MEX AM systems, i.e., ~180-190°C for PLA and ~160-170°C for LDPE and HDPE. The ASTM D638-22 Type I tensile specimens were designed by using Solidworks (Dassault Systèmes, Vélizy-Villacoublay, France), and Simplify 3D was used as slicing software to prepare the corresponding gcode files (Simplify3D, Cincinnati, OH, US). The 3D printing process was managed with OctoPrint [58]. The 3D printing samples were designed with Grasshopper (Rhinoceros, Robert McNeel & Associates, Seattle, WA, US) [59]. The samples reached a maximum nominal dimension of 90x90x90 mm, and nonplanar slicing techniques were used to prepare the gcodes files with Grasshopper. The maximum curvature angle of the extruded path corresponds to 32°, and it considered the physical constraints given by the extruder head, such as the inclination angle of the conic nozzle and the dimensions of the nozzle itself, i.e., ~27 mm (Figure 2b). Comparative planar gcodes were prepared with Simplify 3D as a benchmark to assess the critical overhangs and geometries by using conventional slicing techniques. The visualization of planar and nonplanar gcode paths of the 3D samples was done with NC Viewer [60].

Table. 1 – 3D printing parameters and settings of the 3D printed samples (tensile and 3D samples)

	Parameter/setting	Unit	PLA/SCGs	rLDPE/SCGs	HDPE/SCGs
Tensile samples and 3D samples	Feed rate	mm/s	10	10	10
	T extruder	°C	190	170	170
	T bed	°C	80	80	60
	Adhesion	//	-	Adhesive tape	Adhesive tape
	Nozzle diameter	mm	3	3	3
	Extrusion multiplier	//	2	1.8	1.8
	Extrusion width	mm	4.5	4.5	3.6
	Perimeters	//	1	1	1
3D samples only	3D printing mode	//	Vase mode	Vase mode	Vase mode
	Layer height	mm	0.5, 0.7, 1	0.7, 1	1
	Infill percentage	%	0 (no infill)	0 (no infill)	0 (no infill)
	Curvature angle (nonplanar slicing)	°	0-27°	0-32°	0-22°
Tensile samples only	Layer height	mm	0.5	0.5	0.5
	Infill percentage	%	100	100	100
	Infill type	//	rectilinear	rectilinear	rectilinear

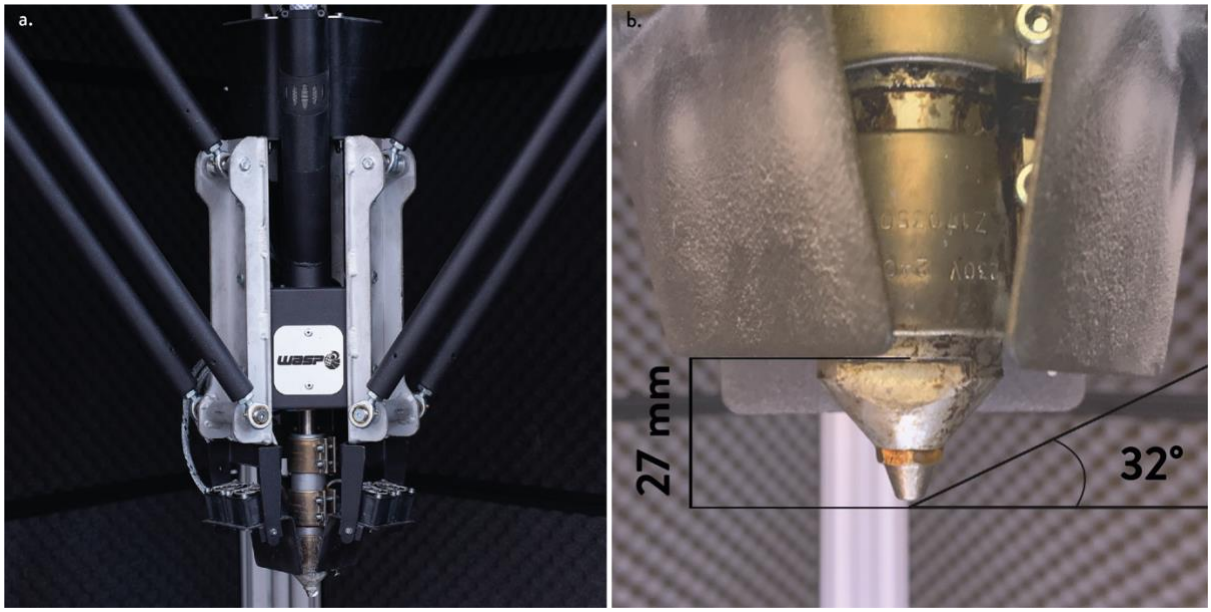


Fig. 2 – 3D printing setup of the large-scale AM system: (a) single screw pellet extruder and (b) insight of the extruder hotend with its main geometrical constraints for nonplanar slicing.

Results and Discussion

Thermal properties

The results of the DSC analysis performed on the three formulations are shown in Table 2 and compared with the main works from the state-of-the-art focusing on PLA- or PE-based formulations with SCGs. The table reports the values of crystallization temperature (T_c) and its enthalpy (ΔH_c) during the cooling ramp, as well as the glass transition temperature (T_g), cold crystallization temperature (T_{cc}), melting temperature (T_m), the enthalpy changes corresponding to the cold crystallization peak (ΔH_{cc}) and melting peak (ΔH_m), and the degree of crystallinity (χ). Two different thermal behaviors were detected for PLA-based and PE-based composites (Figure A1, Appendix). PLA/SCGs showed all states of temperature during the second heating scan. rLDPE/SCGs and HPDE/SCGs only reported a state of melting. The melting temperatures for PLA/SCGs, rLDPE/SCGs, and HDPE/SCGs were found to be 153.5°C, 106.6°C, and 131.5°C, respectively. These values are consistent with the literature and are similar to the ones of the polymer matrixes, as visible in Table 2. Moreover, PLA/SCGs results are comparable with previous examples of 3D printing filaments filled with SCGs, e.g., 59°C of glass temperature [61, 62], and other specific 3D printing grade PLA/SCGs feedstock, e.g., glass and melting temperatures [51], as well as 3D printed PLA [63]. Despite the lack of examples of PE-based composites with SCGs for 3D printing, closed values were found in previous works focused on biomass-based polymer composites for rLDPE/SCGs [64, 65]. Similarly, HDPE/SCGs values are in line with works that combined HDPE matrixes with coffee silverskin and SCGs [28, 66].

However, the degree of crystallinity changed for all three formulations compared to the matrix values from the state-of-the-art, obtaining 7.2 %, 28.3%, and 58.5% for PLA/SCGs, rLDPE/SCGs, and HDPE/SCGs, respectively. For rLDPE and HPDE, decreased values can be due to irregular particle granulometry from SCGs, which can increase crystallization defects, lowering the degree of crystallinity. Focusing on PLA, a slight increase has been previously reported in the state-of-the-art of 3D printing grade PLA/SCGs feedstocks [51, 62], showing a minimal influence of SCGs on the crystallization behavior of similar formulations. Compared to the state-of-the-art, adding SCGs shows limited effects on the thermal behavior of the three formulations. However, it can affect their degree of crystallinity, hence the mechanical properties and failure modes. The values from the thermal analysis helped define possible temperature ranges for the FGF AM process, e.g., extruder and bed temperatures (Table 1) and flow stress ramp tests.

Table. 2 – Thermal properties of PLA/SCGs, rLDPE/SCGs, and HDPE/SCGs from the DSC tests compared with the state-of-the-art of PLA, rLDPE, and HDPE (neat matrix and filled composites).

Formulations	Cooling scan		2nd heating scan					
	T_c (°C)	ΔH_c (J/g)	T_g (°C)	T_{cc} (°C)	ΔH_{cc} (J/g)	T_m (°C)	ΔH_m (J/g)	χ (%)
PLA/SCGs	-	-	59	131.4	5.8	153.5	6.7	7.2
PLA [51]	-	-	61.2	133.6	0.6	154.2	1.9	2.0
PLA/SCGs [51]	-	-	59.5	130.0	6.8	154.0	8.3	8.9
rLDPE/SCGs	90.8	72.3	-	-	-	106.6	82.9	28.3
rLDPE [64]	95	109	-	-	-	112	107	39
rLDPE/SCGs [a]	-	-	-	-	-	-	-	-
HDPE/SCGs	114.7	169.3	-	-	-	131.5	171.5	58.5
HDPE [66]	112.8	190.0	-	-	-	134.1	187.4	63.8
HDPE/SCGs [a]	-	-	-	-	-	-	-	-

[a]= Direct comparison with SCGs currently not available.

Rheological behavior

The flow stress ramp tests were performed at 190°C for PLA/SCGs and 170°C for rLDPE/SCGs and HDPE/SCGs. These values were selected to simulate the thermal conditions of the extruder chamber with the different polymer-based composites, i.e., T extrusion values from Table 1, understanding their printability. Figure 3 shows the flow stress ramp curves on a log-log graph plotting the viscosity as a

function of the shear rate. The curves are non-Newtonian and show a shear-thinning behavior described by the decreasing viscosity at increasing shear rates. The viscosity significantly decreases at shear rates of 10^2 s^{-1}. However, since the pellets were originally produced for injection molding processes, the viscosity values are not optimal for 3D printing, differing from a specific feedstock for 3D printing, i.e., spool filaments for FFF, resulting in different printability [40]. The viscosity values at a shear rate ($\dot{\gamma}$) equal to 27.5 s^{-1}, i.e., simulating the conditions in the extruder chamber during the 3D printing process, are visible in Table 3 [67]. The low values of PLA/SCGs (133.6 Pa·s) and HDPE/SCGs (313.6 Pa·s) highlighted some possible issues in achieving optimal printability. From the literature, low viscosity values correspond to high MFI values, which are generally common for injection molding grade feedstock [68, 69]. Contrarily, extrusion grade pellets have lower MFI values, i.e., >12 g/10min, to help retain the extruded shape and achieve dimensional stability [68, 70]. For MEX AM, feedstocks with ~10-30 g/10min of MFI can be successfully processed [71, 72], reaching intermediate values compared to injection molding and extrusion grade pellets. According to the rheological tests, the viscosity of the three formulations is still comparable with 3D printing feedstocks, as well as their MFI values (Table 3) [73]. This result indicates, at least, a potential processability of the three compounds with this FGF AM system, as then confirmed by the 3D printing tests. According to the state-of-the-art, SCGs can contribute to decreasing the viscosity of the extrudate, making the compounds suitable for 3D printing [33, 51]. In particular, the viscosity of rLDPE/SCGs (839.7 Pa·s) can indicate better printability, as viscosity should be low enough to facilitate the 3D printing process but high enough to provide structural support to ensure dimensional accuracy and shape-retaining [74].

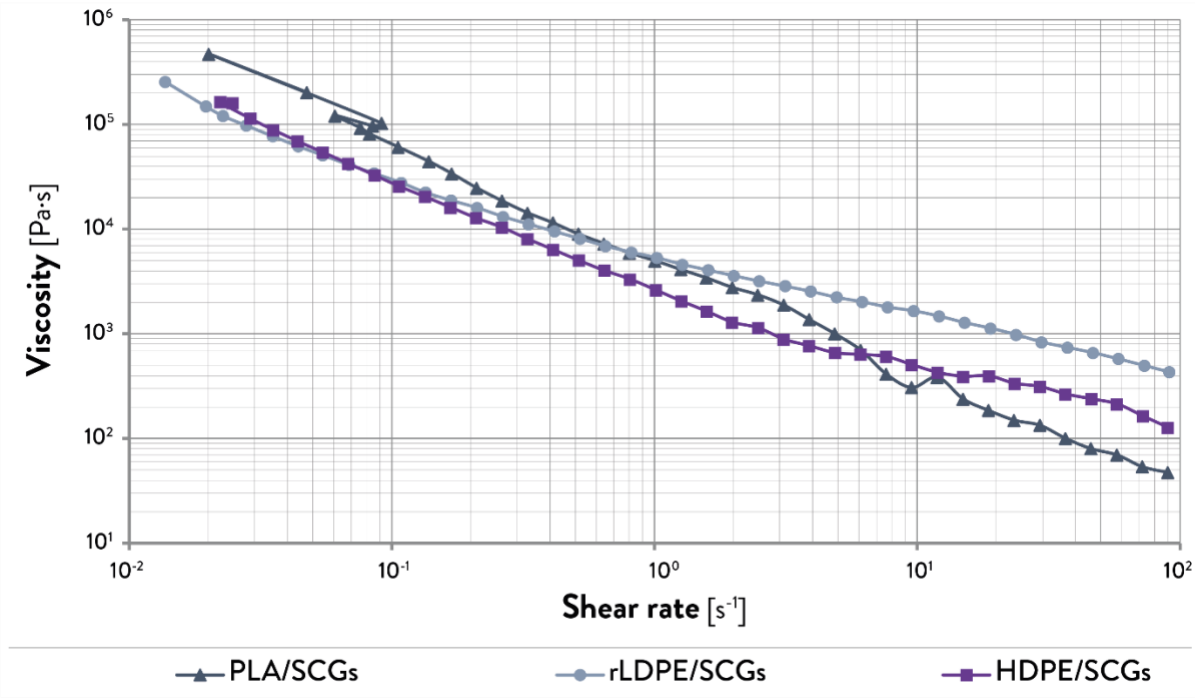


Fig. 3 – Log-log plot of viscosity as a function of the shear rate of PLA/SCGs, rLDPE/SCGs, and HDPE/SCGs.

Table. 3 – Viscosity values when shear rate $\dot{\gamma}$ = 27.5 s^{-1} and Melt Flow Index (MFI) values for PLA/SCGs, rLDPE/SCGs, and HDPE/SCGs.

Formulations	*Viscosity when $\dot{\gamma}$ = 27.5 s^{-1} (Pa·s)*	*MFI (g/10 min)*
PLA/SCGs	133.6	33.5
rLDPE/SCGs	839.7	7.4
HDPE/SCGs	313.6	29.1

Tensile tests

The mechanical properties of the three SCGs polymer-based composites were evaluated through tensile tests on 3D printed samples. Table A1 (Appendix) resumes the values of the elastic modulus (E), the ultimate tensile strength (σ_m), the fracture strength (σ_b), the elongation at maximum strength (ε_m), and the elongation at break (ε_b). Although direct comparisons between PLA- and PE-based formulations filled with SCGs should be avoided, the results from the tensile tests provide an overview of the printability of the three formulations with LFAM FGF apparatuses. In general, PLA/SCGs shows the best accuracy in terms of experimental values, with a relative standard deviation of ~3% for E and ε_m and ~1% for σ_m. rLDPE/SCGs reached values of ~13%, whereas HDPE/SCGs shows the highest variability, i.e., relative standard deviations from ~9% to more than 30%. These results indicate the reliable processability of PLA/SCGs and rLDPE/SCGs with the selected large-format AM FGF apparatus despite their injection molding grade nature. According to the experimental stress-strain curves of Figure 4, the 3D printed specimens exhibited a plastic failure for all three formulations, with accurate yield point values only for PLA/SCGs, i.e., 12.5 ± 0.2 MPa As from Table A1, PLA/SCGs were found to have lower ultimate tensile strength, 13.9 MPa (Figure 5b), and higher elongation at break values, ~3% (Figure 5c), than previous works in literature with 3D printing filaments [33, 62]. This result is in line with the degree of crystallinity obtained from the DSC data (Table 2), decreasing properties such as tensile strength and switching to plastic failure modes. It is mainly due to changes applied to the matrix itself and partly because of the plasticizing effect of SCGs [32]. Since LDPE and HDPE/biomass blends are quite novel compounds for 3D printing, especially using scraps or by-products, HDPE/SCGs cannot be directly compared with previous literature with small- and large-format AM processes. As visible in Figure 5a, rLDPE/SCGs has an elastic modulus mean value of 107.4 MPa. Since the polymer matrix comes from post-industrial recycled feedstock, the overall results report lower mechanical properties compared to virgin material. Despite the lower degree of crystallinity from the DSC data, the tensile properties are still comparable with previous work from literature, which uses rLDPE as a matrix with biomass scraps for extrusion processes [64]. Regarding HDPE/SCGs, the mean values of ultimate tensile strength, 10.9 MPa (Figure 5b), and of elastic modulus, 587 MPa (Figure 5a), are in line with respect to a case study from injection molding [28]. However, slightly lower values were obtained in this case due to the higher presence of voids and defects in the 3D printed samples with the HDPE-based compound, as well as the lower degree of crystallinity compared to the state-of-the-art (Table 2). These results confirm a good printability of rLDPE/SCGs formulation, as well as PLA/SCGs compound, making fully recycled and bio-based formulations for injection molding potential feedstocks for large-format AM. Although HDPE/SCGs samples show more defects and less interlayer adhesion, the mechanical properties are still comparable to conventional processes. Hence, the use of pellet feedstock from conventional processes reduced the steps and costs to obtain secondary raw material, i.e., spool filaments. This fact also helps limit the degradation effects from a further extrusion cycle, expanding the potential feedstocks for applications with LFAM FGF and paving the way for formulations from secondary raw materials [37].

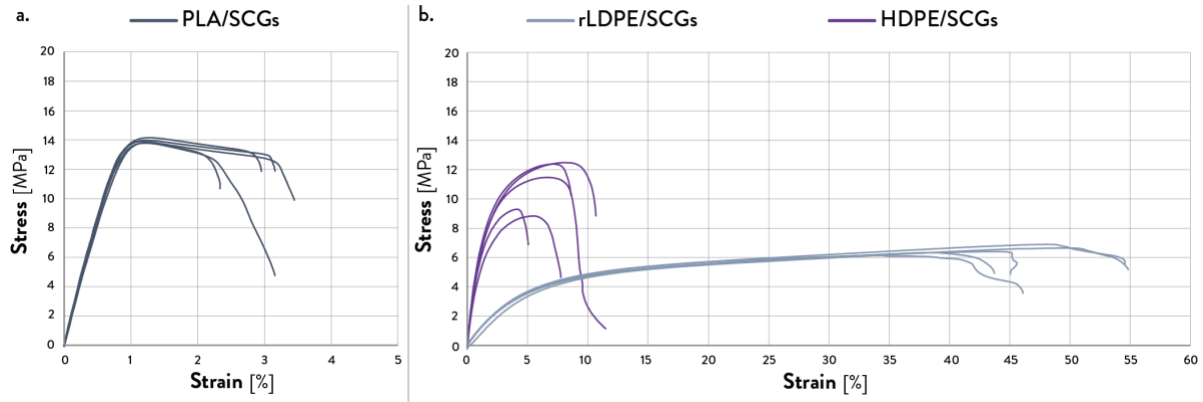


Fig. 4 – Stress-strain curves from the tensile tests: (a) PLA/SCGs; (b) rLDPE/SCGs and HDPE/SCGs.

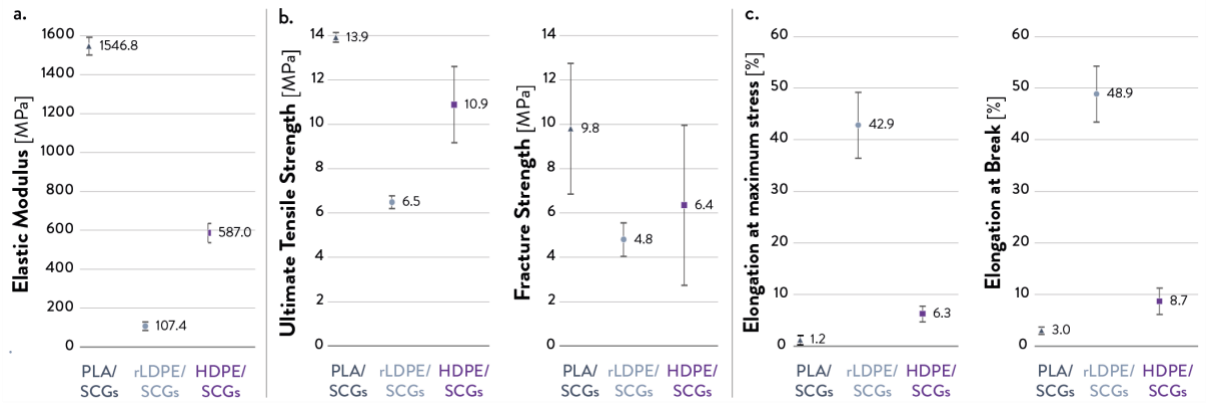


Fig. 5 – Results from the tensile tests: (a) Elastic modulus; (b) Ultimate tensile strength and Fracture strength; and (c) Elongation at maximum stress and Elongation at break.

3D printing tests and nonplanar slicing

The three formulations were 3D printed according to the parameters shown in Table 1, combining the thermal, rheological characterization, and preliminary 3D printing tests to define an optimal set of parameters to be used with the specific LFAM FGF apparatus. In detail, the preliminary 3D printing tests were conducted to evaluate the quality of the extrudate by using extrusion-only gcodes and 3D-printed vase mode cylinders, changing the extruder temperature, feed rate, extrusion multiplier, and extrusion width to reach a consistent extrusion without clogging or obstructions of the screw. These four optimal parameters, reported in Table 1, were then used as a base for fabricating the tensile and 3D nonplanar samples. Similarly, the 3D printed dog bone samples for tensile tests were also used to assess the processability of the different SCGs-based pellet compounds and define other parameters, such as bed temperature. According to Figure 6, the overall quality of the 3D printed samples differs for each processed feedstock. By keeping the same feed rate value, i.e., 10 mm/s, PLA/SCGs (Figure 6a) and rLDPE/SCGs (Figure 6b) reached a consistent flow, resulting in homogeneous extrudate and layer paths. In contrast, the HDPE/SCGs compound (Figure 6c) shows more visible voids and defects, as well as under-extruded areas. In this case, increasing the extrusion width led to frequent clogging, requiring a lower value than the other two formulations (Table 1). Furthermore, rLDPE/SCGs and HDPE/SCGs compounds required further tuning of the 3D printing setup to ensure adhesion, i.e., adapting the bed temperature and using an additional layer of adhesive tape on the bed. Although all three formulations were successfully extruded and processed without failures and clogging, PLA/SCGs and rLDPE/SCGs compounds achieved an overall quality comparable to 3D printing grade feedstock in terms of extrudate consistency and layer path accuracy.



Fig. 6 –3D printed specimens of the three formulations: (a) PLA/SCGs; (b) rLDPE/SCGs; and (c) HDPE/SCGs.

The three formulations were used to fabricate 3D printed samples to assess the printability with complex geometries, e.g., critical overhangs. After fabricating the tensile specimens with conventional planar slicing, non-conventional slicing processes were used to create the gcode files of the samples, i.e., nonplanar slicing. This slicing technique creates curved extrusion paths in the z-axis direction, contrary to planar slicing and common slicing software [47, 48]. Its use can help improve surface quality by

reducing the staircase effect and achieving new freeform or complex geometries by overcoming the constraint of planar cross-sections on the z-axis [75], e.g., overhang collapses. Table 4 resumes the main 3D printing features achievable through nonplanar slicing techniques with the LFAM FGF system, i.e., the minimum and maximum average layer height, curvature angle, and 3D printable overhangs. Samples with a 0.5-1 mm layer height, 32° curvature angle, and 25° overhang were successfully fabricated with the three injection molding grade SCGs-based formulations. Figure 7 shows the three batches of samples made with PLA/SCGs, rLDPE/SCGs, and HDPE/SCGs. The first batch of samples, PLA/SCGs (Figure 7a), was successfully 3D printed at different average layer heights, i.e., 0.5, 0.7, and 1 mm, corresponding to a range between one-sixth and one-third of the nozzle diameter of 3 mm. Different curvature angles were reached when using nonplanar slicing techniques, although some problems in the consistency of the extrudate were observed at 27°, i.e., S4. Higher curvature angles were reached by 3D printing the second sample batch, rLDPE/SCGs (Figure 7b), reaching a maximum angle of 32° and homogeneous extrusion paths, i.e., S4. Finally, the HPDE/SCGs compound (Figure 7c) was successfully 3D printed at an average layer height of 1 mm, combining nonplanar slicing paths with a maximum curvature angle of 22°, i.e., S2. However, S1 exhibited local layer detachment after the 3D printing process, indicating interlayer adhesion issues (Figure 7c). These results are consistent with the rheological behavior studied with the flow stress ramp test, confirming the good printability of rLDPE/SCGs. PLA/SCGs compound was also successfully 3D printed with different average layer heights and curvature angles. Despite the detachment of HDPE/SCGs, good results and better interlayer adhesion can be achieved in terms of extrudate consistency, as visible from S2, Figure 7c.

Table. 4 – Main 3D printing features achievable through nonplanar slicing techniques with the LFAM FGF system and the SCGs-based feedstocks used in this work.

Formulations	Layer height (mm)		Curvature angle (°)	Overhang angle[b] (°)	
	Min	Max	Min	Max	Max
PLA/SCGs	0.5			27	
rLDPE/SCGs	0.7	1	0	32[a]	~25
HDPE/SCGs	1			22	

[a]= This value corresponds to the geometrical limit of the extruder hotend (Figure 2b).
[b]= This parameter is intended as achievable without the need of supports.



Fig. 7 – 3D printed samples with nonplanar slicing techniques: (a) PLA/SCGs; (b) rLDPE/SCGs; and (c) HDPE/SCGs.

Focusing on nonplanar slicing, different curvature angles were tested through the 3D printing tests, i.e., 0-32°, reaching the geometrical constraints of the 3D printing setup. In detail, nonplanar slicing enabled more complex geometrical features, such as challenging overhangs for average layer heights ranging between 0.7 and 1 mm. As visible in Figure 8, nonplanar slicing facilitated the fabrication of some geometries included in the 3D samples through the variation of the curvature angle and layer height [76]. The most intricate overhang features, highlighted with the grey circles, represent some challenging parts to be achieved with planar gcode files, e.g., from conventional slicing software (Figure 8, second row). As visible from the comparison between the planar and nonplanar gcodes, the nonplanar definitions simplified the fabrication of those specific points by locally increasing the curvature angle, decreasing the layer height, and using the previous nonplanar layers to support the next ones. This strategy allowed the fabrication of geometries with a maximum overhang angle of 25° without supports (Table 4). In other words, it reduced the overhang angles of specific parts by locally changing the orientation of the building direction, hence reducing the need of supports for complex overhangs (Figure 8, third row) [48]. In LFAM, avoiding supports is one of the key aspects to consider when designing and producing new parts. They represent a significant source of material waste with large-format AM and big parts, and their removal can cause cracks and damages using big nozzle diameters. Furthermore, nonplanar slicing techniques combined with vase mode helped achieve more accurate 3D printed parts, as visible from the missing path highlighted from the orange areas (Figure 8, second and third row). Although these missing parts can be manufactured without vase mode and building single perimeter walls, nonplanar slicing helps avoid the staircase effect, e.g., reducing post-processing, and vase mode eliminates the need for retractions, which currently represents a critical aspect for FGF systems with big nozzle diameters.

In general, the 3D printed samples validated this approach (Figure 8, fourth row), showing good shape retention and no local collapses close to the overhang areas. Nonplanar slicing can support the use of non-conventional pellet compounds by making overhangs and complex geometries easier to fabricate, avoiding supports, and promoting material waste reduction in a circular economy perspective.

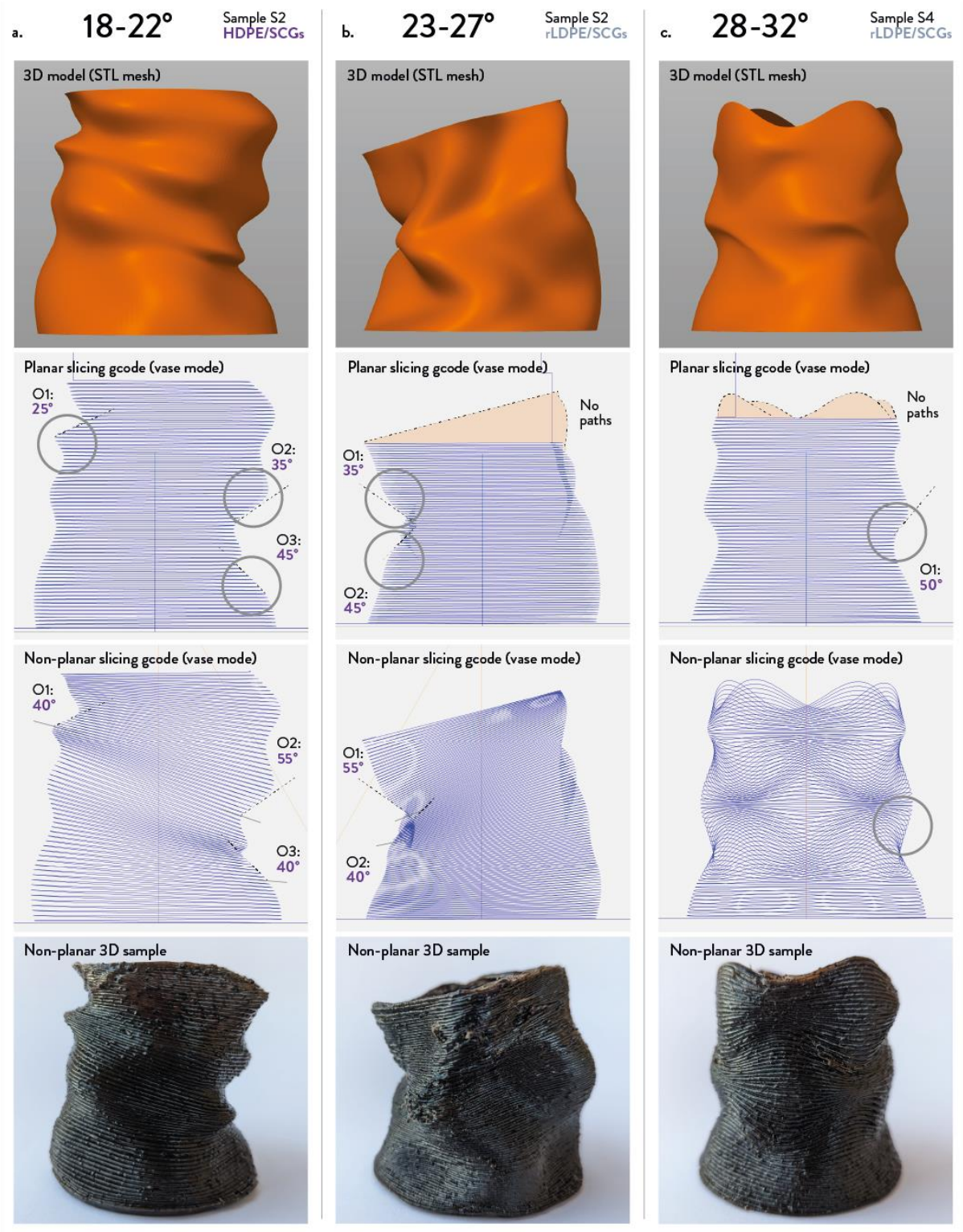


Fig. 8 – Comparison between the 3D model (first row from top), planar gcode (second row), nonplanar gcode (third row), and 3D printed specimens (fourth row) of some sample geometries: samples with (a) 18-22° curvature angle; (b) 23-27° curvature angle; and (c) 28-32° curvature angle (geometrical limit of the LFAM FGF 3D printer). The scheme highlights critical overhang angles to be achieved with planar slicing (grey circles, indicated as "O" and numbered in the second and third rows) and missing paths with planar vase mode (orange areas in the second row).

Potential applications, limitations, and future developments

According to the results from the 3D printing tests, rLDPE/SCGs and PLA/SCGs can be potentially used for new large-format products with 3D printing, especially considering the current scarcity of granulate feedstock for LFAM from biomass scraps and by-products [41, 50]. For instance, furniture represents an emerging and growing sector for biomass waste-based polymer compounds for 3D printing [41]. rLDPE/SCGs and PLA/SCGs formulations can be a potential option for large-format customized products, e.g., tables and seats [51]. Nonplanar slicing can support the use of similar biomass-based compounds for complex geometries without the need for supports, hence reducing material waste and enlarging the range of achievable shapes for new products, e.g., interior design elements, freeform facades, or temporary exhibition stands. In contrast, HDPE/SCGs compound shows promising results for medium-size customized products, such as accessories, furnishing, and packaging. However, their processing should be further optimized to be used for such applications, mainly to improve the interlayer adhesion and printability, e.g., using a rheological modifier. In this case, a 3D printing grade formulation can also be studied to improve its processability for LFAM FGF processes, especially considering the limited availability of HDPE-based feedstock for this technology.

Despite the achieved results with injection molding grade feedstocks, this research currently lacks a comparison with similar 3D printing grade pellets in terms of characterization and printability, as well as with the three pure polymer matrixes or other LFAM FGF apparatuses. In addition, 3D printing tests with alternative geometries and a large-format part are currently missing and should be carried out to further demonstrate the process reliability and strengthen the results from this work, e.g., a sample application from the furniture sector [51]. Future work can focus on the in-depth investigation of other 3D printing parameters, such as infill percentage and pattern, increasing the versatility of LFAM FGF in terms of achievable geometries. Similarly, the impact of specific 3D printing process parameters should be explored through comprehensive experimentation, e.g., focusing on layer height and flow rate. It can be carried out starting from the most promising formulations from this study, rLDPE/SCGs and PLA/SCGs, paving the way for their use in real contexts through a case study investigation. Additional investigation can be done by further narrowing down on materials characterization, e.g., assessing the matrixes and filler degradation or comparing the commercial feedstock composites with the pure matrixes used for compounding. Other biomass-based compound formulations can also be studied for LFAM FGF, both 3D printing and injection molding grade, enlarging the available materials for the market. In addition, other applications can be developed and fabricated with similar LFAM systems, e.g., through a real case study in collaboration with companies and design studios, defining some guidelines for using similar feedstocks in real-world contexts. Finally, further work can be done to assess and analyze the potential recyclability and reusability of these compounds for multiple fabrication cycles or other manufacturing processes, fostering a wider approach to circular design through LFAM. Large-format 3D printing can potentially enlarge the range of applications for biomass waste-based polymer compounds, offering a wider choice of materials by using pellets from conventional processes without any further reprocessing step on the secondary raw material, i.e., extruding spool filaments.

Conclusions

In this work, three commercial polymer-based compounds filled with SCGs from injection molding were characterized for LFAM FGF systems and 3D printed to achieve self-supported complex geometries through nonplanar slicing. The experimentation aimed to enlarge the range of available materials for LFAM pellet extrusion 3D printing processes with biomass scraps or by-products, as well as pave the way for new product applications. The thermal, rheological, and mechanical properties of PLA/SCGs, rLDPE/SCGs, and HDPE/SCGs injection molding grade pellet compounds were investigated to assess their printability through DSC, flow stress ramp tests, and tensile tests, respectively. The overall quality from the LFAM FGF process was assessed through 3D printed samples with different average layer heights and complex overhang geometries, also obtained through nonplanar slicing. According to the characterization, the thermal behavior of SCGs-based formulations is

comparable with other formulations from the literature, e.g., melting temperatures of 154.2°C (PLA/SCGs), 106.6°C (rLDPE/SCGs), and 131.5°C (HDPE/SCGs), defining some temperature ranges for their processability with the 3D printing system, i.e., 190°C for PLA/SCGs and 170°C for rLDPE/SCGs and HDPE/SCGs. Although the compounds are injection molding grade feedstock, their viscosity values, ranging between 133.6 and 839.7 Pa·s, indicate the potential use for 3D printing processes, especially rLDPE/SCGs. Tensile tests on the 3D printed specimens confirm the feasibility of using novel SCGs polymer-based feedstock, i.e., rLDPE or HDPE. The tests show quite accurate results for PLA/SCGs and rLDPE/SCGs formulations in terms of relative standard deviation, up to ~1-3% and ~5-14%. Despite the low degree of crystallinity, comparable results with conventional manufacturing processes were found for rLDPE/SCGs, e.g., 107.4 MPa of elastic modulus, and HDPE/SCGs, e.g., 10.9 MPa of ultimate tensile strength and 587 MPa of elastic modulus. The printability was then assessed by successfully fabricating different 3D printing samples, simplifying the achievement of critical overhangs through nonplanar slicing, i.e., angles up to 25° and maximum nonplanar curvature of 32°, avoiding the need for supports. Commercial injection molding grade SCG-filled compounds can be successfully processed with LFAM FGF technologies, especially rLDPE/SCGs and PLA/SCGs, paving the way for new large-format applications, i.e., furniture products, customized interior elements, or temporary exhibition stands. Although other types of geometries and the impact of specific 3D printing parameters should be tested to support real implementations, these three formulations represent viable options for large-format 3D printing without requiring specific 3D printing grade material. The most promising results were achieved with PLA/SCGs and rLDPE/SCGs compounds, a bio-based formulation and a fully recycled material, respectively. Further work should be carried out to (a) optimize the use of HDPE for large-format applications by reducing the printability and interlayer adhesion issues, (b) study real-case applications, and (c) analyze the potential recyclability and reusability of these polymer-based compounds, following circular economy approaches. Nevertheless, a more comprehensive range of materials from biomass scraps and by-products can be successfully used with large-format 3D printing systems, achieving complex shapes. Using pellet-based extrusion heads also fosters possible scaling-up solutions by reducing the need for specific 3D printing grade feedstock and costs and impacts related to their reprocessing, i.e., extrusion of filaments. To conclude, this study paves the way to study, develop, and use novel biomass-based pellet or granulate feedstock for LFAM, as well as 3D printing strategies, e.g., nonplanar slicing, promoting material waste reduction and circular economy practices.

Ethics approval and consent to participate – Not applicable.
Consent for publication – Not applicable.
Availability of data and materials – Data are available on request from the authors.
Competing interests – Not applicable.
Funding – This research received no external fundings.

Authors' contributions
All co-authors contributed to the research and the drafting of the publication. A.R. and M.P. equally contributed to the work. All authors read and approved the final manuscript.

Acknowledgements
The authors would like to acknowledge Nexeo Plastics Italy S.r.l. for providing the compounded pellets of the three formulations tested in this work.

Appendix

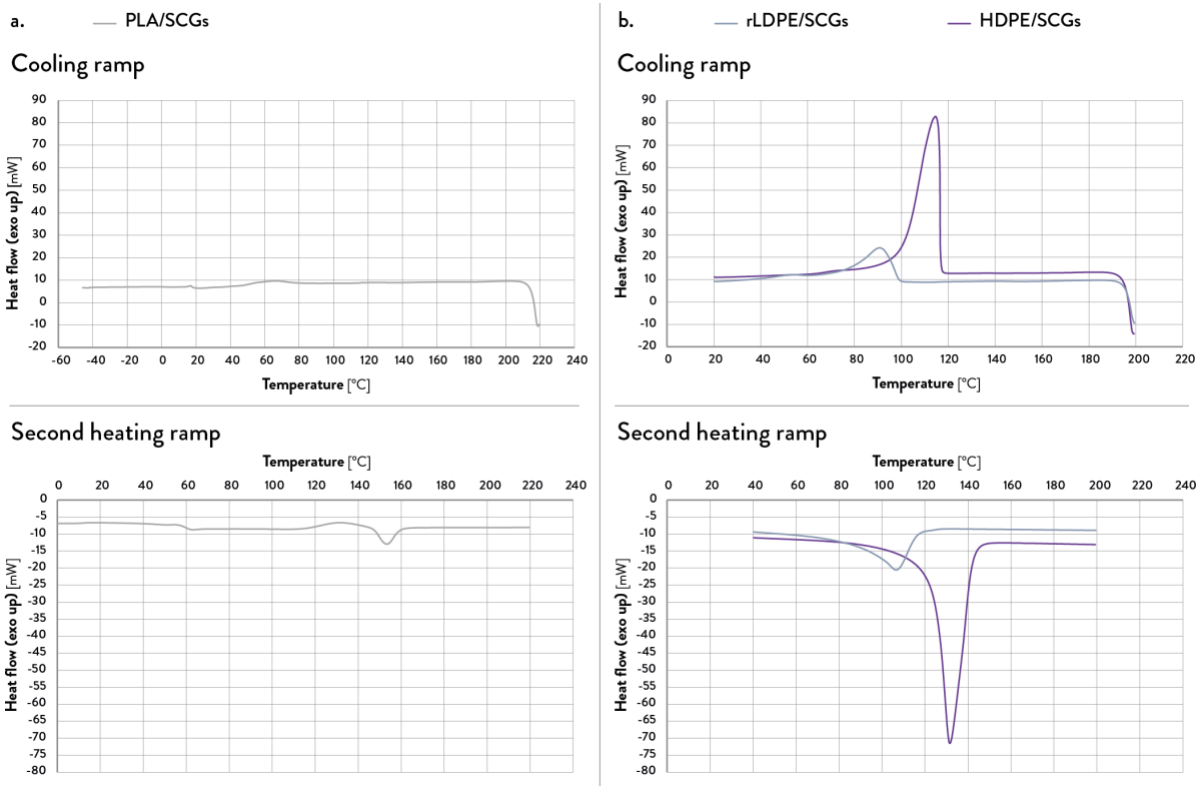


Fig. A1 – DSC curves (Cooling ramp and second heating ramp) of: (a) PLA/SCGs; (b) rLDPE/SCGs, and HDPE/SCGs.

Table A1 – Values of experimental elastic modulus, yield strength, ultimate tensile strength, fracture strength, elongation at maximum stress, and elongation at break with the corresponding standard deviation and relative standard deviation (in brackets).

Formulations	E (MPa)	σ_y (MPa)	σ_m (MPa)	σ_b (MPa)	ε_m (%)	ε_b (%)
PLA/SCGs	1546.8 ± 45.5 (2.9%)	12.5 ± 0.2 (1.7%)	13.9 ± 0.1 (1.1%)	9.8 ± 2.9 (30.1%)	1.2 ± 0.1 (3.3%)	3 ± 0.4 (13.8%)
rLDPE/SCGs	107.4 ± 14.3 (13.3%)	1.1 ± 0.3 (26.1%)	6.5 ± 0.3 (4.5%)	4.8 ± 0.8 (15.7%)	42.9 ± 6.4 (14.9%)	48.9 ± 5.4 (11.1%)
HDPE/SCGs	587 ± 49.7 (8.5%)	5.4 ± 0.7 (12.3%)	10.9 ± 1.7 (15.8%)	6.4 ± 3.6 (56.7%)	6.3 ± 1.5 (24.4%)	8.7 ± 2.5 (29.2%)

References

1. (2021) UNEP Food Waste Index Report 2021. In: UNEP - UN Environment Programme. http://www.unep.org/resources/report/unep-food-waste-index-report-2021. Accessed 14 Jul 2023
2. (2015) The 17 Sustainable Development Goals (SDGs) - United Nations. https://sdgs.un.org/goals. Accessed 28 Jul 2021
3. Intergovernmental Panel on Climate Change (IPCC) (2022) Climate Change and Land: IPCC Special Report on Climate Change, Desertification, Land Degradation, Sustainable Land Management, Food Security, and Greenhouse Gas Fluxes in Terrestrial Ecosystems. Cambridge University Press, Cambridge
4. Bomfim ASC de, de Oliveira DM, Walling E, et al (2023) Spent Coffee Grounds Characterization and Reuse in Composting and Soil Amendment. Waste 1:2–20. https://doi.org/10.3390/waste1010002
5. Coffee | International Coffee Organization. https://icocoffee.org/coffee-/. Accessed 24 Jul 2023
6. Gebreeyessus GD (2022) Towards the sustainable and circular bioeconomy: Insights on spent coffee grounds valorization. Sci Total Environ 833:155113. https://doi.org/10.1016/j.scitotenv.2022.155113
7. Kourmentza C, Economou ChN, Tsafrakidou P, Kornaros M (2018) Spent coffee grounds make much more than waste: Exploring recent advances and future exploitation strategies for the valorization of an emerging food waste stream. Journal of Cleaner Production 172:980–992. https://doi.org/10.1016/j.jclepro.2017.10.088
8. Nab C, Maslin M (2020) Life cycle assessment synthesis of the carbon footprint of Arabica coffee: Case study of Brazil and Vietnam conventional and sustainable coffee production and export to the United Kingdom. Geo: Geography and Environment 7:e00096. https://doi.org/10.1002/geo2.96
9. Ellen MacArthur Foundation (EMF) (2013) Towards the Circular Economy
10. Geissdoerfer M, Savaget P, Bocken NMP, Hultink EJ (2017) The Circular Economy – A new sustainability paradigm? J Clean Prod 143:757–768. https://doi.org/10.1016/j.jclepro.2016.12.048
11. Reike D, Vermeulen WJV, Witjes S (2018) The circular economy: New or Refurbished as CE 3.0? — Exploring Controversies in the Conceptualization of the Circular Economy through a Focus on History and Resource Value Retention Options. Resour Conserv Recycl 135:246–264. https://doi.org/10.1016/j.resconrec.2017.08.027
12. Neves A, Godina R, Azevedo SG, Matias JCO (2020) A comprehensive review of industrial symbiosis. Journal of Cleaner Production 247:119113. https://doi.org/10.1016/j.jclepro.2019.119113
13. Usmani Z, Sharma M, Karpichev Y, et al (2020) Advancement in valorization technologies to improve utilization of bio-based waste in bioeconomy context. Renewable and Sustainable Energy Reviews 131:109965. https://doi.org/10.1016/j.rser.2020.109965
14. Carus M, Dammer L (2018) The Circular Bioeconomy—Concepts, Opportunities, and Limitations. Ind Biotechnol 14:83–91. https://doi.org/10.1089/ind.2018.29121.mca
15. Bioeconomy. In: European Commission. https://ec.europa.eu/info/research-and-innovation/research-area/environment/bioeconomy_en. Accessed 4 Jul 2022
16. Cao D (2023) Investigation into surface-coated continuous flax fiber-reinforced natural sandwich composites via vacuum-assisted material extrusion. Prog Addit Manuf. https://doi.org/10.1007/s40964-023-00508-6
17. Cao D (2023) Fusion joining of thermoplastic composites with a carbon fabric heating element modified by multiwalled carbon nanotube sheets. Int J Adv Manuf Technol 128:4443–4453. https://doi.org/10.1007/s00170-023-12202-6
18. Hassan M, Mohanty AK, Misra M (2023) 3D Printing in Upcycling Plastic and Biomass Waste to Sustainable Polymer Blends and Composites: A Review. Materials & Design 112558. https://doi.org/10.1016/j.matdes.2023.112558
19. Holden NM, Neill AM, Stout JC, et al (2022) Biocircularity: a Framework to Define Sustainable, Circular Bioeconomy. CircEconSust. https://doi.org/10.1007/s43615-022-00180-y
20. Muscat A, de Olde EM, Ripoll-Bosch R, et al (2021) Principles, drivers and opportunities of a circular bioeconomy. Nat Food 2:561–566. https://doi.org/10.1038/s43016-021-00340-7
21. Balla VK, Tadimeti JGD, Sudan K, et al (2021) First report on fabrication and

characterization of soybean hull fiber: polymer composite filaments for fused filament fabrication. Prog Addit Manuf 6:39–52. https://doi.org/10.1007/s40964-020-00138-2
22. Dey A, Rahman MM, Gupta A, et al (2023) A Performance Study on 3D-Printed Bioplastic Pots from Soybean By-Products. Sustainability (Switzerland) 15:. https://doi.org/10.3390/su151310535
23. Gama N, Magina S, Barros-Timmons A, Ferreira A (2021) Enhanced compatibility between coconut fibers/PP via chemical modification for 3D printing. Prog Addit Manuf. https://doi.org/10.1007/s40964-021-00226-x
24. Vieira F, Santana HEP, Jesus M, et al (2024) Coconut Waste: Discovering Sustainable Approaches to Advance a Circular Economy. Sustainability 16:3066. https://doi.org/10.3390/su16073066
25. Saberian M, Li J, Donnoli A, et al (2021) Recycling of spent coffee grounds in construction materials: A review. Journal of Cleaner Production 289:125837. https://doi.org/10.1016/j.jclepro.2021.125837
26. McNutt J, He Q (Sophia) (2019) Spent coffee grounds: A review on current utilization. Journal of Industrial and Engineering Chemistry 71:78–88. https://doi.org/10.1016/j.jiec.2018.11.054
27. Sohn JS, Ryu Y, Yun C-S, et al (2019) Extrusion Compounding Process for the Development of Eco-Friendly SCG/PP Composite Pellets. Sustainability 11:1720. https://doi.org/10.3390/su11061720
28. Mendes JF, Martins JT, Manrich A, et al (2021) Thermo-physical and mechanical characteristics of composites based on high-density polyethylene (HDPE) e spent coffee grounds (SCG). J Polym Environ 29:2888–2900. https://doi.org/10.1007/s10924-021-02090-w
29. Cacciotti I, Mori S, Cherubini V, Nanni F (2018) Eco-sustainable systems based on poly(lactic acid), diatomite and coffee grounds extract for food packaging. International Journal of Biological Macromolecules 112:567–575. https://doi.org/10.1016/j.ijbiomac.2018.02.018
30. Garcia CV, Kim Y-T (2021) Spent Coffee Grounds and Coffee Silverskin as Potential Materials for Packaging: A Review. J Polym Environ 29:2372–2384. https://doi.org/10.1007/s10924-021-02067-9
31. ASTM International (2015) ISO/ASTM 52900-15 Standard Terminology for Additive Manufacturing – General Principles – Terminology. ASTM International, West Conshohocken, PA
32. Chang Y-C, Chen Y, Ning J, et al (2019) No Such Thing as Trash: A 3D-Printable Polymer Composite Composed of Oil-Extracted Spent Coffee Grounds and Polylactic Acid with Enhanced Impact Toughness. ACS Sustainable Chem Eng 7:15304–15310. https://doi.org/10.1021/acssuschemeng.9b02527
33. Yu IKM, Chan OY, Zhang Q, et al (2023) Upcycling of Spent Tea Leaves and Spent Coffee Grounds into Sustainable 3D-Printing Materials: Natural Plasticization and Low-Energy Fabrication. ACS Sustainable Chem Eng 11:6230–6240. https://doi.org/10.1021/acssuschemeng.2c07330
34. Cao D, Bouzolin D, Lu H, Griffith DT (2023) Bending and shear improvements in 3D-printed core sandwich composites through modification of resin uptake in the skin/core interphase region. Composites Part B: Engineering 264:110912. https://doi.org/10.1016/j.compositesb.2023.110912
35. Anwajler B, Zdybel E, Tomaszewska-Ciosk E (2023) Innovative Polymer Composites with Natural Fillers Produced by Additive Manufacturing (3D Printing)—A Literature Review. Polymers 15:. https://doi.org/10.3390/polym15173534
36. Romani A, Caba S, Suriano R, Levi M (2023) Recycling Glass and Carbon Fibers for Reusable Components in the Automotive Sector through Additive Manufacturing. Applied Sciences 13:5848. https://doi.org/10.3390/app13105848
37. Nieto DM, Molina SI (2019) Large-format fused deposition additive manufacturing : a review. Rapid Prototyp J. https://doi.org/10.1108/RPJ-05-2018-0126
38. Vicente CMS, Sardinha M, Reis L, et al (2023) Large-format additive manufacturing of polymer extrusion-based deposition systems: review and applications. Prog Addit Manuf 8:1257–1280. https://doi.org/10.1007/s40964-023-00397-9
39. Alexandre A, Cruz Sanchez FA, Boudaoud H, et al (2020) Mechanical Properties of Direct Waste Printing of Polylactic Acid with Universal Pellets Extruder: Comparison to Fused Filament Fabrication on Open-Source Desktop Three-Dimensional Printers. 3D Print Addit Manuf 7:237–247. https://doi.org/10.1089/3dp.2019.0195

40. Khaliq MH, Gomes R, Fernandes C, et al (2017) On the use of high viscosity polymers in the fused filament fabrication process. Rapid Prototyping Journal 23:727–735. https://doi.org/10.1108/RPJ-02-2016-0027
41. Romani A, Suriano R, Levi M (2023) Biomass waste materials through extrusion-based additive manufacturing: A systematic literature review. J Cleaner Prod 386:135779. https://doi.org/10.1016/j.jclepro.2022.135779
42. Chesser P (2019) Extrusion control for high quality printing on Big Area Additive Manufacturing (BAAM) systems. Addit Manuf 28:445-455,. https://doi.org/10.1016/j.addma.2019.05.020.
43. Justino Netto JM, Idogava HT, Frezzatto Santos LE, et al (2021) Screw-assisted 3D printing with granulated materials: a systematic review. Int J Adv Manuf Technol 115:2711–2727. https://doi.org/10.1007/s00170-021-07365-z
44. Kishore V, Ajinjeru C, Nycz A, et al (2017) Infrared preheating to improve interlayer strength of big area additive manufacturing (BAAM) components. Additive Manufacturing 14:7–12. https://doi.org/10.1016/j.addma.2016.11.008
45. Meraz Trejo E, Jimenez X, Billah KMM, et al (2020) Compressive deformation analysis of large area pellet-fed material extrusion 3D printed parts in relation to in situ thermal imaging. Additive Manufacturing 33:101099. https://doi.org/10.1016/j.addma.2020.101099
46. D'Amico T, Peterson AM (2020) Bead parameterization of desktop and room-scale material extrusion additive manufacturing: How print speed and thermal properties affect heat transfer. Additive Manufacturing 34:101239. https://doi.org/10.1016/j.addma.2020.101239
47. Nisja GA, Cao A, Gao C (2021) Short review of nonplanar fused deposition modeling printing. Mat Des Process Commun mdp2.221. https://doi.org/10.1002/mdp2.221
48. Nayyeri P, Zareinia K, Bougherara H (2022) Planar and nonplanar slicing algorithms for fused deposition modeling technology: a critical review. Int J Adv Manuf Technol 119:2785–2810. https://doi.org/10.1007/s00170-021-08347-x
49. Bhatt PM, Malhan RK, Shembekar AV, et al (2020) Expanding capabilities of additive manufacturing through use of robotics technologies: A survey. Additive Manufacturing 31:100933. https://doi.org/10.1016/j.addma.2019.100933
50. Sanchez FAC, Boudaoud H, Camargo M, Pearce JM (2020) Plastic recycling in additive manufacturing: A systematic literature review and opportunities for the circular economy. J Clean Prod 264:. https://doi.org/10.1016/j.jclepro.2020.121602.
51. Paramatti M, Romani A, Pugliese G, Levi M (2024) PLA feedstock filled with spent coffee grounds for new product applications with large-format Material Extrusion Additive Manufacturing. ACS Omega 9:6423–6431. https://doi.org/10.1021/acsomega.3c0566
52. Ngo TD, Kashani A, Imbalzano G, et al (2018) Additive manufacturing (3D printing): A review of materials, methods, applications and challenges. Compos Part B: Eng 143:172–196. https://doi.org/10.1016/j.compositesb.2018.02.012
53. Fischer EW, Sterzel HJ, Wegner G (1973) Investigation of the structure of solution grown crystals of lactide copolymers by means of chemical reactions. Kolloid-Z.uZPolymere 251:980–990. https://doi.org/10.1007/BF01498927
54. Lei Y, Wu Q, Clemons CM, et al (2007) Influence of nanoclay on properties of HDPE/wood composites. Journal of Applied Polymer Science 106:3958–3966. https://doi.org/10.1002/app.27048
55. Chhabra RP (2010) Non-Newtonian Fluids: An Introduction. In: Krishnan JM, Deshpande AP, Kumar PBS (eds) Rheology of Complex Fluids. Springer, New York, NY, pp 3–34
56. Giles HF, Wagner JR, Mount EM (2005) 7 - Scale Up. In: Giles HF, Wagner JR, Mount EM (eds) Extrusion. The Definitive Processing Guide and Handbook. William Andrew Publishing, Norwich, NY, pp 75–77
57. American Society for Testing and Materials (2021) ASTM D638-14: Standard Test Method for Tensile Properties of Plastics
58. Häußge G OctoPrint.org. In: OctoPrint.org. https://octoprint.org/. Accessed 23 Jun 2023
59. Cuevas DDG, Pugliese DG (2020) Advanced 3D Printing with Grasshopper®: Clay and FDM. Independently published, Wrocław
60. Luciano X (2018) NC Viewer // GCode Viewer and Machine Simulator. https://ncviewer.com/. Accessed 21 Dec 2023

61. Li S, Shi C, Sun S, et al (2021) From brown to colored: Polylactic acid composite with micro/nano-structured white spent coffee grounds for three-dimensional printing. International Journal of Biological Macromolecules 174:300–308. https://doi.org/10.1016/j.ijbiomac.2021.01.176
62. Yu W, Yuan T, Yao Y, et al (2023) PLA/Coffee Grounds Composite for 3D Printing and Its Properties. Forests 14:367. https://doi.org/10.3390/f14020367
63. Romani A, Perusin L, Ciurnelli M, Levi M (2024) Characterization of PLA feedstock after multiple recycling processes for large-format material extrusion additive manufacturing. Materials Today Sustainability 25:100636. https://doi.org/10.1016/j.mtsust.2023.100636
64. Pedroso AG, Rosa DS (2005) Mechanical, thermal and morphological characterization of recycled LDPE/corn starch blends. Carbohydrate Polymers 59:1–9. https://doi.org/10.1016/j.carbpol.2004.08.018
65. Gupta A, Mohanty AK, Misra M (2022) Biocarbon from spent coffee ground and their sustainable biocomposites with recycled water bottle and bale wrap: A new life for waste plastics and waste food residues for industrial uses. Composites Part A: Applied Science and Manufacturing 154:106759. https://doi.org/10.1016/j.compositesa.2021.106759
66. Hejna A, Barczewski M, Kosmela P, et al (2021) Coffee Silverskin as a Multifunctional Waste Filler for High-Density Polyethylene Green Composites. Journal of Composites Science 5:44. https://doi.org/10.3390/jcs5020044
67. Geri T (2020) Printability funnel: rheological and thermo-mechanical studies for Big Area Additive Manufacturing parameters assessment. Politecnico di Milano
68. Polychronopoulos ND, Vlachopoulos J (2018) Polymer Processing and Rheology. In: Jafar Mazumder MA, Sheardown H, Al-Ahmed A (eds) Functional Polymers. Springer International Publishing, Cham, pp 1–47
69. Shenoy AV, Saini DR, Nadkarni VM (2006) Melt Rheology of Polymer Blends from Melt Flow Index. International Journal of Polymeric Materials. https://doi.org/10.1080/00914038408080271
70. Tsai H-H, Wu S-J, Wu Y-D, Hong W-Z (2022) Feasibility Study on the Fused Filaments of Injection-Molding-Grade Poly(Ethylene Terephthalate) for 3D Printing. Polymers 14:2276. https://doi.org/10.3390/polym14112276
71. Wang S, Capoen L, D'hooge DR, Cardon L (2018) Can the melt flow index be used to predict the success of fused deposition modelling of commercial poly(lactic acid) filaments into 3D printed materials? Plastics, Rubber and Composites 47:9–16. https://doi.org/10.1080/14658011.2017.1397308
72. Doronin F, Rudakova A, Rytikov G, Nazarov V (2023) Simple Determination of the Melt Flow Index of Composite Polymer Filaments Used in Material Extrusion Additive Manufacturing. Coatings 13:1592. https://doi.org/10.3390/coatings13091592
73. Patti A, Acierno S, Cicala G, Acierno D (2023) Predicting the Printability of Poly(Lactide) Acid Filaments in Fused Deposition Modeling (FDM) Technology: Rheological Measurements and Experimental Evidence. ChemEngineering 7:1. https://doi.org/10.3390/chemengineering7010001
74. Lay M, Thajudin NLN, Hamid ZAA, et al (2019) Comparison of physical and mechanical properties of PLA, ABS and nylon 6 fabricated using fused deposition modeling and injection molding. Composites Part B: Engineering 176:107341. https://doi.org/10.1016/j.compositesb.2019.107341
75. Ahlers D, Wasserfall F, Hendrich N, Zhang J (2019) 3D Printing of Nonplanar Layers for Smooth Surface Generation. In: IEEE 15th International Conference on Automation Science and Engineering (CASE). pp 1737–1734
76. Mitropoulou I, Bernhard M, Dillenburger B (2022) Nonplanar 3D Printing of Bifurcating Forms. 3D Printing and Additive Manufacturing 9:189–202. https://doi.org/10.1089/3dp.2021.0023